

Maximum likelihood inference for high-dimensional problems with multiaffine variable relations [★]

Jean-Sébastien Brouillon ^a, Florian Dörfler ^b, Giancarlo Ferrari-Trecate ^a

^a*Institute of Mechanical Engineering, École Polytechnique Fédérale de Lausanne, Switzerland*

^b*Automatic Control Laboratory, Swiss Federal Institute of Technology (ETH), Switzerland*

Abstract

Maximum Likelihood Estimation of continuous variable models can be very challenging in high dimensions, due to potentially complex probability distributions. The existence of multiple interdependencies among variables can make it very difficult to establish convergence guarantees. This leads to a wide use of brute-force methods, such as grid searching and Monte-Carlo sampling and, when applicable, complex and problem-specific algorithms. In this paper, we consider inference problems where the variables are related by multiaffine expressions. We propose a novel Alternating and Iteratively-Reweighted Least Squares (AIRLS) algorithm, and prove its convergence for problems with Generalized Normal Distributions. We also provide an efficient method to compute the variance of the estimates obtained using AIRLS. Finally, we show how the method can be applied to graphical statistical models. We perform numerical experiments on several inference problems, showing significantly better performance than state-of-the-art approaches in terms of scalability, robustness to noise, and convergence speed due to an empirically observed super-linear convergence rate.

Key words: maximum likelihood estimation, identification methods, estimation theory, nonlinear models, Bayesian networks

1 Introduction

Statistical inference is widely used in many disciplines such as environmental sciences, economics, energy systems, and control theory (Nojavan et al., 2017; Qian and Miltner, 2015; Xu et al., 2020; Borunda et al., 2016; Carbonari et al., 2014). More precisely, inference allows learning and predicting model variables from noisy observations, sometimes also providing a measure of the predictive uncertainty. However, fitting a model to data generally leads to complex inference problems. Furthermore, specific variables of interest often need to be estimated although some latent (unobserved) variables are unknown.

Among inference methods, Maximum Likelihood Estimation (MLE) is very popular for its consistency

and efficiency properties (Lehmann and Casella, 2006; Griliches et al., 1983). The computation of MLE estimates can be fairly simple for problems where few variables need to be inferred, but becomes much harder when their numbers increase (Murphy, 2012). Rather than inferring the value of latent variables, one can marginalize the likelihood over them, like in Expectation-Maximization (EM). Marginalizations may improve the estimation accuracy, but are often not tractable when the latent variables are high-dimensional or do not take discrete values (Saul, 2020).

In MLE, if the probability distributions of all continuous variables are Gaussian, the likelihood can often be maximized using standard convex optimization techniques such as Gradient Descent (GD) and ADMM (Boyd et al., 2011). Additionally, several methods have been developed for problems where the relations between the Gaussian random variables follow complex graph structures (Hellman et al., 2012; McGeachie et al., 2014; Hu and Mahadevan, 2018). More generally, proximal methods and Iteratively Reweighted Least Squares (IRLS) provide a simple adaptation to Generalized Normal Distributions (GNDs, also called exponential power distributions), but only in specific cases (Beck, 2017).

[★] This research is supported by the Swiss National Science Foundation under the NCCR Automation (grant agreement 51NF40-180545).

Email addresses: jean-sebastien.brouillon@epfl.ch (Jean-Sébastien Brouillon), dorfler@control.ee.ethz.ch (Florian Dörfler), giancarlo.ferraritrecate@epfl.ch (Giancarlo Ferrari-Trecate).

Moreover, current methods focus on problems where all GNDs have the same exponent, which amount to minimizing a norm.

Many inference problems contain multiaffine relations between GND-distributed random variables. For example, the unknown parameters in both Error-In-Variables (EIV) and rank-constrained tensor regression models relate in a multi-linear way (Llosa, 2018; Zhou et al., 2013). Signal processing and system identification problems can also present multiaffine relations, e.g., when unknown filter or system parameters multiply with unmeasured disturbances (Gibson and Ninness, 2005; Söderström, 2018). Additionally, Livadiotis (2020) have shown that adapting the exponent of GNDs to a problem can substantially improve the goodness of fit.

The aforementioned challenges explain why almost all practical MLE methods for complex problems are based on Monte Carlo sampling and discretization (i.e., grid search) (Chen et al., 2017; Monti and Cooper, 2013; Kroese et al., 2013). Although these two approaches are simple to implement and provide an approximate probability distribution for the estimates, they are dependent on the sampling distributions or discretization strategies used, which may impact the estimation accuracy (Chen et al., 2017). The computational complexity of these methods, growing rapidly with both the desired accuracy and the dimension of the problem, is the most important limitation, which prevents their use in many applications. Other zeroth-order methods such as the Gradient-Less Descent (GLD) can help to reduce the computational burden in high dimensions, but display slow convergence (Golovin et al., 2019).

The contributions of this paper are fourfold. First, we present an efficient algorithm, called Alternating and Iteratively-Reweighted Least Squares (AIRLS), for MLE with multiaffine-related variables. Second, we prove the convergence of AIRLS if each variable follows a GND. Moreover, we discuss the optimality of the likelihood of the estimate for finite-precision solvers, showing that the suboptimality decays with the solver’s precision. Third, we describe a method to obtain the confidence intervals of the MLE estimates. This last step is particularly useful because, while MLE provides estimates, it is often hard to compute their precision given by the Cramer-Rao lower bound (Lehmann and Casella, 2006). This bound depends on the likelihood evaluated at the ground truth, and can be very sensitive to uncertainty when using estimates instead of (unknown) exact values. Fourth and finally, all the contributions are substantiated by extensive simulations on various problems from different scientific fields. Empirical evidence shows that AIRLS converges to a meaningful estimate even when the distributions are not restricted to GNDs. The main algorithm is implemented in a custom developed open source package (Brouillon, 2022), which provides an easy-to-use interface for MLE problems with multiaffine

related variables faster than with other aforementioned methods. Application-specific versions of the AIRLS algorithm were presented in Brouillon et al. (2022a) and Brouillon et al. (2022b). Compared to the previous works, this paper considers a much wider class of likelihoods, presents a deeper theoretical analysis of the algorithm’s convergence, and provide tools to evaluate the quality of the final estimates.

The paper is organized as follows. Section 2 states the inference problem and Section 3 presents our algorithm. Section 4 discusses the optimality of the result’s likelihood. Section 5 shows how to compute the estimate’s variance. Section 6 is devoted to numerical examples and Section 7 concludes the paper.

1.1 Preliminaries and notations

The operator $\text{diag}(\cdot)$ creates a diagonal matrix from the elements of a vector. The j^{th} row of a matrix X is denoted by X_j and the j^{th} column by $X_{:j}$. For n scalars or row vectors X_1, \dots, X_n , $[X_i]_{i=1}^n$ corresponds to the matrix or vector constructed by vertically stacking X_1, \dots, X_n . For a vector $x = [x_j]_{j=1}^{n_B}$ composed of n_B blocks, the vector x_{-i} is the vector of all blocks but the i^{th} . The 2-norm of a vector or the spectral norm of a matrix is denoted by $\|\cdot\|$. The norm of a vector x weighted by a positive definite matrix W is denoted by $\|x\|_W = \sqrt{x^\top W x}$. The ℓ_1 norm is $\|x\|_1$. The Moore-Penrose pseudoinverse of a matrix X is X^\dagger . The function $\text{sgn}(\cdot) \in \{-1, 1\}$ gives the sign of a real number and we set $\text{sgn}(0) = 1$ by definition.

The expectation and covariance matrix of a random variable $x \in \mathbb{R}^n$ are denoted by $\mathbb{E}[x] \in \mathbb{R}^n$ and $\mathbb{V}[x] \in \mathbb{R}^{n \times n}$, respectively. The empirical variance of the elements of a vector $x \in \mathbb{R}^n$ is given by $\text{Var}[x] = \frac{1}{n^2} (n x^\top x - (\sum_{i=1}^n x_i)^2) \in \mathbb{R}$.

Definition 1 (Multiaffine function) *Let x_1, \dots, x_{n_B} be a decomposition of x into $n_B \geq 1$ blocks, where the blocks $x_i \in \mathbb{R}^{n_i}$ are nonempty disjoint subsets of the scalar variables composing x such that their union gives x . A scalar function $g(x)$ is called multiaffine if $g(x)$ depends on any single block x_i in an affine way.*

A vector field $R(x) = [g_1(x), \dots, g_M(x)]^\top \in \mathbb{R}^M$ is multiaffine if and only if each element g_i is multiaffine with respect to the same decomposition $x = [x_1^\top, \dots, x_{n_B}^\top]^\top$.

As an example of block definitions, the vector $x^\top = \underbrace{[x_1, x_2]}_{x_{b1}}, \underbrace{[x_3]}_{x_{b1}}, \underbrace{[x_4, x_5, x_6, x_7]}_{x_{b3}}$ can be decomposed into 3 blocks x_{b1} , x_{b2} , and x_{b3} .

Example 2 *The function $g : \mathbb{R}^3 \rightarrow \mathbb{R}, g_{\text{multi}}(x) = x_1 x_2 x_3 + x_1 - x_3 + 1$ is multiaffine with respect to the de-*

composition $x = [x_1^\top, x_2^\top, x_3^\top]^\top$, while $g_{sq}(x) = x_1x_2 - x_2^2$ is not multiaffine due to the squared variable.

Since, by definition, each element of G depends on a single block of variables x_i in an affine way, one has the following result.

Corollary 1 For a multiaffine vector field $R : \mathbb{R}^{\sum_{i=1}^{n_B} n_i} \rightarrow \mathbb{R}^M$, the following n_B equalities simultaneously hold.

$$R(x) = C_i(x_{-i}) - F_i(x_{-i}) \cdot x_i, \quad \forall i \in \{1, \dots, n_B\}, \quad (1)$$

where $F_i(x_{-i}) \in \mathbb{R}^{M \times n_i}$ and $C_i(x_{-i}) \in \mathbb{R}^M$ are suitable functions.

Corollary 1 provides a trivial linearization with respect to each block x_i , which is exploited in the sequel to simplify the computations. For example, the function g_{multi} from Example 2 can be written as

$$\begin{aligned} x_1x_2x_3 + x_1 - x_3 + 1 &= x_1 \underbrace{(x_2x_3 + 1)}_{F_i(x_{-1})} - \underbrace{x_3 + 1}_{C_i(x_{-1})}, \\ &= x_2 \underbrace{(x_1x_3)}_{F_i(x_{-2})} + \underbrace{x_1 - x_3 + 1}_{C_i(x_{-2})}, \\ &= x_3 \underbrace{(x_1x_2 - 1)}_{F_i(x_{-3})} + \underbrace{x_1 + 1}_{C_i(x_{-3})}. \end{aligned}$$

Definition 3 A standard GND has a density function given by

$$p_h(y) = \frac{q_h^{1+q_h}}{2\Gamma(q_h^{-1})} e^{-q_h|y|^{q_h}}, \quad (2)$$

where Γ is the Gamma function and $q_h \in \mathbb{R}_+$ is a positive parameter.

The class of standard GNDs includes the standard normal ($q_h = 2$) and Laplace ($q_h = 1$) distributions, as well as the uniform distribution on $[-1, 1]$ as a limit case for $q_h \rightarrow \infty$ (Nadarajah, 2005). Note that q_h is not limited to integers but can be any positive real number (see Sections 6.3 and 6.4).

2 Problem statement

The paper focuses on MLE problems where the joint probability distribution has the following structure.

Assumption 1 The joint probability density $p(x)$ is proportional to the product of $p_1(r_1(x)), \dots, p_M(r_M(x))$ of M GNDs with exponents $q_h \leq \bar{q} \in \mathbb{N}$. The functions $r_h(x)$ for $h = 1, \dots, M$ are multiaffine functions with respect to the same decomposition x_1, \dots, x_{n_B} .

Example 4 The distribution $p(x) \propto e^{-(x_1x_2x_3)^2} \cdot e^{-|x_1+x_2x_3|}$ satisfies Assumption 1. Indeed, $p(x)$ is proportional to the product of the densities $p_1(g_1(x)) \propto e^{-g_1(x)^2}$ and $p_2(g_2(x)) \propto e^{-|g_2(x)|}$, where $g_1(x) = x_1x_2x_3$ and $g_2(x) = x_1 + x_2x_3$ are both multiaffine with respect to the decomposition $x = [x_1^\top, x_2^\top, x_3^\top]^\top$.

Although the limitation to GNDs might seem restrictive, these distributions are quite common in engineering applications and other distributions can often be approximated with their product. For example, the truncated normal distribution is the product between a normal and a uniform distribution, both of which can be obtained from (2) with $q_h = 2$ and $q_h \rightarrow \infty$, respectively. Additionally, multiaffine models are a generalization of linear ones, and can model complex problems in many fields such as Bayesian and EIV system identification (Söderström, 2018; Bottegal et al., 2014; Ninness and Henriksen, 2010; Chiuso, 2016), Generalized Kalman smoothing in signal processing (Aravkin et al., 2017), and generalized principal component analysis and tensor regressions in machine learning (Vidal et al., 2005; Magni et al., 1998; Guhaniyogi et al., 2017; Llosa, 2018). In particular, the three following examples have quite simple solutions when the uncertainty is Gaussian-distributed, but can become quite computationally intensive when any GNDs are considered. The detailed derivations are given in the Appendix.

Example 5 (Generalized PCA) Fitting a set of n subspaces defined by their normal vectors x_i amounts to solving $\prod_{i=1}^n \phi_h^\top x_i = \epsilon_h \approx 0$ for all data points ϕ_h with $h = 1, \dots, M$, in the noise-free case. If the residuals ϵ_h follow a distribution p , the most likely fit is given in (Vidal et al., 2005) by

$$\arg \max_{x_1, \dots, x_n} \prod_{h=1}^M p \left(\prod_{i=1}^n \phi_h^\top x_i \right).$$

Example 6 (EIV System Identification) Let $Z_1 \in \mathbb{R}^{T \times n}$ and $Z_2 \in \mathbb{R}^{T \times n}$ be the stacked matrices of noisy measurement of the states of a system from $t = 0$ to $t = T - 1$ and $t = 1$ to $t = T$, respectively, and let X_1 and X_2 be their exact value. From (Söderström, 2018), if the measurements of the states are independent, the maximum-likelihood inference of the matrix $X_0 \in \mathbb{R}^{n \times n}$ relating X_1 and X_2 as $X_2 = X_1X_0$ can be written as

$$\arg \max_{X_0, X_1} \prod_{h,t=1}^{n,T} p_{th} \left(Z_{2th} - \sum_{i=1}^n X_{1th} X_{0hi} \right) p_{t-1,h} (X_{1th} - Z_{1th}),$$

where p_{th} is the probability distribution of the measurement error of the state h at time t .

Example 7 (Low rank tensor regressions) Linear regression models $Z = \Phi X$ are common in ma-

chine learning. However, Z and Φ may be quite large or high-order tensors in problems such as imaging (Guhaniyogi et al., 2017). It is therefore sometimes necessary to find a lower-rank representation, e.g., in 2 dimensions and with rank 1, $X = x_1 x_2^\top$ where $x_1 \in \mathbb{R}^{n_1}$ and $x_2 \in \mathbb{R}^{n_2}$. This gives the following maximum likelihood estimation problem

$$\arg \max_{x_1, x_2} \prod_{h,t=1}^{n_1, T} p_{th} \left(Z_{th} - \sum_{i=1}^{n_2} x_{1h} x_{2i} \Phi_{ti} \right),$$

where p_{ht} is the probability distribution of the element (t, h) of the matrix of residuals $Z - \Phi X$.

More generally, many nonlinear functions can also be expressed as a multiaffine function using a change of variable $x = [\psi_1(v_1), \dots, \psi_{n_B}(v_{n_B})]$, where v is the initial variable and ψ_i are nonlinear function. This amounts to learning the coefficients of the basis functions of a model. More examples are provided in Section 6.4.

Using Assumption 1, maximizing the probability of the variables x amounts to solve

$$\arg \max_x \prod_{h=1}^M p_h(r_h(x)), \quad (3)$$

where the probability densities p_h and multiaffine functions r_h satisfy Assumption 1. Note that since all functions $r_h(x)$ are multiaffine with respect to the same decomposition, they can be written as the element of a multiaffine vector field $R(x)$ defined in (1). Moreover, Corollary 1 allows one to split the problem (3) into multiple sub-problems in order to build an iterative method and to ensure that the likelihood maximization is tractable. In the sequel, we will focus on optimizing the negative log-likelihood

$$G(x) = - \sum_{h=1}^M \log p_h(r_h(x)), \quad (4)$$

instead of (3). This operation yields the same optimizer and is commonly done in the MLE literature.

The problem (3) provides the intuition that, similar to more classical regression model fitting problems based on Least Squares, MLE aims to minimize all the scalar residuals

$$r_h(x) = f_{h1}(x_{-1})x_1 - c_{h1}(x_{-1}), \quad (5a)$$

$$\begin{aligned} & \vdots \\ & = f_{hn_B}(x_{-n_B})x_{n_B} - c_{hn_B}(x_{-n_B}), \end{aligned} \quad (5b)$$

where $f_{hi}(x_{-i})$, and $c_{hi}(x_{-i})$ are the h^{th} elements of $F_i(x_{-i})$ and $C_i(x_{-i})$, respectively. Likewise, we define the

modified residuals $\hat{\rho}_h(x)$ as

$$\hat{\rho}_h(x) = \text{sgn}(r_h(x))(r_h(x)^2 + \alpha)^{\frac{1}{q}}, \quad (6)$$

where $\text{sgn}(x)$ is the sign function and $\alpha > 0$ is a small real constant. This modification is central to the numerical stability of the AIRLS algorithm presented in the sequel.

3 AIRLS Algorithm

Naively, one could solve (3) by nesting two existing techniques: (i) IRLS, which is very popular in problems with non-Gaussian distribution (e.g., logistic or Laplace) and (ii) Block Coordinate Descent (BCD), which is often used to solve problems with multiaffine costs (Kümmerle et al., 2020; de Leeuw, 1994). Such a nested approach would require IRLS to converge at each iteration of BCD, which would be quite slow for high dimensional problems. To alleviate this high computational complexity, we propose to execute only one iteration of (i) and (ii), alternatingly. The pseudo-code for such an approach is given in Algorithm 1.

Algorithm 1 AIRLS

Require: $\alpha > 0$, $x_{\text{init}} \in \mathbb{R}^n$

$x \leftarrow x_{\text{init}}$, $\mathcal{L}_- = \infty$, $\mathcal{L}_+ = - \sum_{h=1}^M \log p_h(\hat{\rho}_h(x_{\text{init}}))$

while $\mathcal{L}_- - \mathcal{L}_+ > \text{tol}$ **do**

for $i = 1, \dots, n_B$ **do**

$$W(x) = \text{diag} \left(\frac{\log \frac{p_1(0)}{p_1(\hat{\rho}_1(x))}}{|\hat{\rho}_1(x)|^q}, \dots, \frac{\log \frac{p_M(0)}{p_M(\hat{\rho}_M(x))}}{|\hat{\rho}_M(x)|^q} \right) \quad (7)$$

$$x_i \leftarrow (F_i(x_{-i})^\top W(x) F_i(x_{-i}))^\dagger F_i(x_{-i})^\top W(x) C_i(x_{-i}) \quad (8)$$

end for

$\mathcal{L}_- = \mathcal{L}_+$, $\mathcal{L}_+ = - \sum_{h=1}^M \log p_h(\hat{\rho}_h(x))$

end while

In words, Algorithm 1 consists of approximating problem (3) with the quadratic problem

$$\arg \min_{x'_i} \|C_i(x_{-i}) - F_i(x_{-i})x'_i\|_{W(x)}^2, \quad (9)$$

w.r.t. one of the variable blocks x_i , and to use the closed-form solution (8) to iteratively update x_i . Next, we address the convergence of Algorithm 1. Although it belongs to the class of reformulation-linearization algorithms, it is not obvious that the specific implementation for (3) converges (Dalkiran and Sherali, 2016; Piccalo et al., 2022).

A main result of this paper is to show that Algorithm 1 converges, as stated in the following theorem. Specifically, the proof of the theorem shows that the following

map $\hat{G}(x)$ decreases at each iteration.

$$\hat{G}(x) = G(0) + \sum_{h=1}^M \left((r_h(x))^2 + \alpha \right)^{\frac{q_h}{\bar{q}}}, \quad (10)$$

where $q_h \leq \bar{q}$ is the exponent of p_h . The weights $W(x)$ are designed such that the quadratic cost in (9) is equal to $\hat{G}(x)$ when $x'_i = x_i$ and $\alpha = 0$. The convergence only relies on a small numerical stability parameter $\alpha > 0$, which avoids singularities if some residuals actually decay to zero.

Theorem 1 (Convergence) *Under Assumption 1, Algorithm 1 converges to a fixed point.*

Proof. For space reasons, in this proof, we will only write W_i , C_i , and F_i instead of $W(x_i, x_{-i})$, $C_i(x_{-i})$, and $F_i(x_{-i})$, respectively. Note that $\alpha > 0$ is required for W_i to be finite, and Assumption 1 allows one to define C_i and F_i . The update (8) is equivalent to

$$\begin{aligned} W_i^{\frac{1}{2}}(C_i - F_i x_i^+) &= W_i^{\frac{1}{2}} R(x^+) \\ &= W_i^{\frac{1}{2}} R(x) - W_i^{\frac{1}{2}} F_i (F_i^\top W_i F_i)^\dagger F_i^\top W_i^{\frac{1}{2}} W_i^{\frac{1}{2}} R(x), \end{aligned} \quad (11)$$

where $R(x)$ is defined in (1) and x and $x^+ = [x_{-i}, x_i^+]^\top$ denote the variables before and after the update, respectively. The matrix $P_i = I_{n_i} - W_i^{\frac{1}{2}} F_i (F_i^\top W_i F_i)^\dagger F_i^\top W_i^{\frac{1}{2}}$ is an orthogonal projection matrix because $P_i^2 = P_i = P_i^\top$. Hence, the norm $\|W_i^{\frac{1}{2}} R(x)\|_2^2 = \|R(x)\|_{W_i}^2$ does not increase with the update (8). Note that $W_i \succ 0$ because $\alpha > 0$ and $\text{sgn}(0) = 1$. Writing this decrease in norm term by term yields

$$\sum_{h=1}^M \underbrace{\log \frac{p_h(0)}{p_h(\hat{\rho}_h(x))}}_{w_h(x)} (r_h(x^+))^2 \leq \sum_{h=1}^M \log \frac{p_h(0)}{p_h(\hat{\rho}_h(x))} (r_h(x))^2.$$

We can add $w_h(x)\alpha$ to both sides of the inequality to transform $(r_h(x))^2$ into $|\hat{\rho}_h(x)|^{\bar{q}}$ and obtain

$$\sum_{h=1}^M \frac{|\hat{\rho}_h(x^+)|^{\bar{q}}}{|\hat{\rho}_h(x)|^{\bar{q}}} \log \frac{p_h(0)}{p_h(\hat{\rho}_h(x))} \leq \sum_{h=1}^M \frac{|\hat{\rho}_h(x)|^{\bar{q}}}{|\hat{\rho}_h(x)|^{\bar{q}}} \log \frac{p_h(0)}{p_h(\hat{\rho}_h(x))}.$$

Since p_h is a GND of exponent q_h , $\log \frac{p_h(0)}{p_h(\hat{\rho}_h(x))} = |\hat{\rho}_h(x)|^{q_h}$. Hence, the inequality becomes

$$\sum_{h=1}^M |\hat{\rho}_h(x^+)|^{\bar{q}} |\hat{\rho}_h(x)|^{q_h - \bar{q}} \leq \sum_{h=1}^M |\hat{\rho}_h(x)|^{q_h}. \quad (12)$$

We can now relate the left-hand side term to $\hat{G}(x^+)$ using Young's inequality $ab \leq \frac{a-1}{q} a^{\frac{q}{q-1}} + \frac{1}{q} b^q$, where $a = 1$,

$b = \frac{|\hat{\rho}_h(x^+)|^{q_h}}{|\hat{\rho}_h(x)|^{q_h}}$, and $q = \frac{\bar{q}}{q_h} \geq 1$. When both sides are multiplied by $|\hat{\rho}_h(x)|^{q_h}$, this yields

$$\begin{aligned} |\hat{\rho}_h(x^+)|^{q_h} &= 1 \frac{|\hat{\rho}_h(x^+)|^{q_h}}{|\hat{\rho}_h(x)|^{q_h}} \cdot |\hat{\rho}_h(x)|^{q_h} \\ &\leq \frac{\bar{q} - q_h}{\bar{q}} |\hat{\rho}_h(x)|^{q_h} + \frac{q_h}{\bar{q}} |\hat{\rho}_h(x^+)|^{\bar{q}} |\hat{\rho}_h(x)|^{q_h - \bar{q}}, \end{aligned} \quad (13)$$

which holds with equality if and only if $|\hat{\rho}_h(x)| = |\hat{\rho}_h(x^+)|$. One can recognize the terms of the left-hand side of (12) on the right-hand side of (13). Hence, by summing (13) over all $h = 1, \dots, M$, one obtains that $\sum_{h=1}^M |\hat{\rho}_h(x^+)|^{q_h} \leq \sum_{h=1}^M |\hat{\rho}_h(x)|^{q_h}$, or equivalently, that $\hat{G}(x)$ decreases at every iteration.

We continue the proof by showing the existence of a compact positive invariant set of the algorithm. First, we split x as $x^\parallel + x^\perp = [x_i^\parallel]_{i=1}^{n_B} + [x_i^\perp]_{i=1}^{n_B}$, where, for all $i = 1, \dots, n_B$, $x_i^\parallel \in \text{range}(F_i)$ and $x_i^\perp \in \text{null}(F_i)$. Second, we make the following observations.

- (i) While x_{-i} is not modified by a single update (9), any element of both x^\parallel and x^\perp may vary.
- (ii) In general, $\|x^\parallel\|_2$ is bounded by a constant $x_{\max} < +\infty$ because $\hat{G}(x)$ is radially unbounded with respect to x^\parallel and must be lesser than $\hat{G}(x_{\text{init}})$.
- (iii) After an update (8) for any i , x_i^\parallel belongs to (9) and $x_i^\parallel = 0$ because $\text{null}((F_i^\top W_i F_i)^\dagger) = \text{null}(F_i)$.

Third, (iii) implies $\|x_i\|_2 = \|x_i^\parallel\|_2$. Hence, (ii) implies that $\|x_i\|_2 \leq \|x^\parallel\|_2 \leq x_{\max}$ always holds after the update (8) of x_i for all $i = 1, \dots, n_B$. Fourth and finally, despite (i), the bound on $\|x_i\|_2$ implies that $\|x\|_2 \leq \|x_{\text{init}}\|_2 + n_B x_{\max}$, which means that the ball of radius $\|x_{\text{init}}\|_2 + n_B x_{\max}$ is a forward invariant for Algorithm 1.

To conclude the proof, we consider Algorithm 1 as an autonomous discrete-time system with state x , a compact positive invariant set, and a positive-semidefinite function $\hat{G}(x)$ that decreases over any state trajectory. LaSalle's invariance principle therefore proves the existence a set of accumulation points to which x converges. Furthermore, $\hat{G}(x) = \hat{G}(x^+)$ can only hold if (12) holds with equality, i.e., if $W_i^{-\frac{1}{2}} P_i W_i^{\frac{1}{2}} R(x) = R(x)$, which is only satisfied if $x_i = (F_i^\top W_i F_i)^\dagger F_i^\top W_i C_i$. For x to be in the set of accumulation points, the equality in must hold for all i , meaning that x is a fixed point, which concludes the proof. \square

Algorithm 1 requires a numerical stability parameter α to avoid a division by zero if some residuals are zero. This parameter depends on the machine precision. To tune it, one can start with the baseline floating point

precision (e.g., $2.22 \cdot 10^{-16}$ with 64 bits under the IEEE-754 standard), and increase α until the solution stops changing significantly. In what follows, we denote the fixed point to which AIRLS converges by \hat{x} . The next section will discuss the magnitude of the approximation introduced by α .

4 Suboptimality bound for heavy-tailed distributions

The convergence of Algorithm 1 does not necessarily guarantee that the fixed point is an optimizer of (3), due to the approximation introduced by the numerical stability parameter α . As α increases, the accuracy of the approximation (9) of the minimizer of (4) decreases. In what follows, we quantify the suboptimality introduced by α when $\bar{q} = 2$.

Assumption 2 *The problem (3) has a unique critical point, which is its maximum.*

Assumption 2, which is used only in this section, is not very restrictive given that the distributions p_h are already unimodal. It is verified when the multiaffine functions inside all p_h are sufficiently different, i.e., if one $r_i(x)$ takes the same value at different points, some other $r_j(x)$ with $j \neq i$ must take different values on these points. Under Assumption 2, one can characterize the suboptimality of a fixed point \hat{x} of Algorithm 1 using the map $\hat{G}(x)$, defined in (10). The following Lemma shows that Algorithm 1 actually minimizes $\hat{G}(x)$ rather than $G(x)$ defined in (4).

Lemma 1 *Under Assumption 1, any fixed point \hat{x} of Algorithm 1 is a critical point of the function $\hat{G}(x)$.*

Proof. The proof starts by computing the gradient of each term of (10). We have

$$\nabla_{x_i} \hat{G}(x) = \sum_{h=1}^M f_{hi}(x_{-i}) \cdot 2r_h(x) \cdot \frac{q_h}{\bar{q}} (r_h(x)^2 + \alpha)^{\frac{q_h}{\bar{q}} - 1}. \quad (14)$$

If all p_h are standard GNDs, the elements of the weight matrix $W(x)$ defined in (7) can be written as

$$W_h(x) = q_h ((f_{ih}(x_{-i}) \cdot x_i - c_{ih}(x_{-i}))^2 + \alpha)^{\frac{q_h}{\bar{q}} - 1}. \quad (15)$$

By simplifying (14) and writing it in matrix form using (15), we have

$$\nabla_{x_i} \hat{G}(x) = \frac{2}{\bar{q}} F_i(x_{-i})^\top W(x) (F_i(x_{-i}) x_i - C_i(x_{-i})). \quad (16)$$

Combining (16) with (9), we observe that at a fixed point of Algorithm 1, $\nabla_{x_i} \hat{G}(x) \Big|_{x=\hat{x}} = \mathbf{0}_{n_i}$ for all i , which concludes the proof. \square

Since Algorithm 1 optimizes \hat{G} , we are interested to derive bounds on the difference between G and \hat{G} . This can be done for $\bar{q} = 2$, i.e., when the distributions are heavy-tailed.

Lemma 2 *Under Assumption 1 and if $\bar{q} = 2$, $G(x)$ satisfies*

$$\hat{G}(x) \geq G(x) \geq \hat{G}(x) - \sum_{h=1}^M \alpha^{\frac{q_h}{2}}, \quad \forall x \in \mathbb{R}^n. \quad (17)$$

Proof. The first inequality $\hat{G}(x) \geq G(x)$ holds because both $\alpha > 0$ and $q_h > 0$. The second inequality is obtained by rewriting $\hat{G}(x)$ as

$$G(0) + \sum_{h=1}^M \frac{r_h^2(x)}{(r_h^2(x) + \alpha)^{1 - \frac{q_h}{2}}} + \frac{\alpha}{(r_h^2(x) + \alpha)^{1 - \frac{q_h}{2}}}. \quad (18)$$

The function $G(x)$ can also be rewritten as $G(x) = G(0) + \sum_{h=1}^M r_h^2(x) (r_h^2(x))^{\frac{q_h}{2} - 1}$ if p_h follows Definition 3, which is greater than the first term of (18) because the denominator is smaller as α is positive. Hence,

$$G(x) \geq \hat{G}(x) - \alpha (r_h^2(x) + \alpha)^{\frac{q_h}{2} - 1}. \quad (19)$$

Since $r_h^2(x) \geq 0$, (17) holds true. \square

Using both the optimality of the fixed points \hat{x} for \hat{G} and the bounds on the difference between G and \hat{G} , we can evaluate the optimality of these fixed points.

Theorem 2 *Under Assumption 1 and 2 and if $\bar{q} = 2$, the corresponding fixed point \hat{x} of Algorithm 1 is a ϵ -suboptimal estimate of the minimum of $G(x)$, i.e.,*

$$|G(\hat{x}) - \min_x G(x)| \leq \epsilon = \sum_{h=1}^M \alpha^{\frac{q_h}{2}}. \quad (20)$$

Proof. Let x^* be the exact minimum of $G(x)$. Assumption 2 implies that, similar to G , \hat{G} also has only one critical point, which is a minimum. Therefore, Lemmas 1 and 2 show that,

$$G(\hat{x}) \underbrace{\leq}_{\text{Lemma 2}} \hat{G}(\hat{x}) \underbrace{\leq}_{\text{Lemma 1}} \hat{G}(x^*) \underbrace{\leq}_{\text{Lemma 2}} G(x^*) + \sum_{h=1}^M \alpha^{\frac{q_h}{2}}.$$

Moreover, by definition $G(x^*) \leq G(\hat{x})$. Hence, combining all the inequalities yields

$$G(x^*) \leq G(\hat{x}) + \sum_{h=1}^M \alpha^{\frac{q_h}{2}},$$

which implies (20) and proves the theorem. \square

5 Error variance estimation

By definition, the exact solution x^* of the problem (3) is the realization of a random variable x such that $r_h(x) \sim p_h$ for all $h = 1, \dots, n_B$ and $i = 1, \dots, M$. Hence, any estimate \hat{x}_i has a statistical error \hat{e}_i , defined as the difference of \hat{x}_i and its ground truth. As the MLE is unbiased under very weak assumptions (Griliches et al., 1983), the expected error $\mathbb{E}[\hat{e}_i]$ is often zero. In this section, we aim to characterize the variance of the estimation error \hat{e}_i .

A common approach to solve this problem is to compute the corresponding Fischer information matrix (Murphy, 2012), which is obtained by differentiating the likelihood defined for the MLE problem. This implies that this method can only be used when all p_h are sufficiently smooth.

A more generally applicable method to obtain confidence intervals for point estimates such as the MLE is random resampling (e.g., Jackknife, Bootstrapping) (Lehmann and Casella, 2006). For all $i = 1, \dots, n_B$, this approach consists of generating many samples $\hat{x}_i^{(k)}$, $k = 1, \dots, N_S$ of x_{-i} according to the distributions p_h evaluated at the MLE estimate \hat{x}_{-i} , and solve (4) N_S times for x_i . The variations of the corresponding solutions $\hat{x}_i^{(k)}$ with respect to the error in \hat{x}_{-i} allow one to evaluate the empirical variance

$$\mathbb{V}[\hat{x}_i] = \sum_{k=1}^{N_S} \frac{\hat{x}_i^{(k)} (\hat{x}_i^{(k)})^\top}{N_S^2} - \left(\sum_{k=1}^{N_S} \frac{\hat{x}_i^{(k)}}{N_S} \right) \left(\sum_{k=1}^{N_S} \frac{\hat{x}_i^{(k)}}{N_S} \right)^\top, \quad (21)$$

which gives $\mathbb{V}[\hat{e}_i] = \mathbb{V}[\hat{x}_i]$. Resampling methods are very popular due to their ease of implementation and reliability. However, as the inference problem must be solved N_S times, a variance estimate is at least N_S times more computationally expensive than the point estimate.

In the following proposition, we exploit the least-squares structure of the iterations of Algorithm 1 to obtain an estimate of $\mathbb{V}[\hat{e}_i]$ without solving the inference problem for each sample. We use the compact notations $W_i^{(k)}$, $C_i^{(k)}$, and $F_i^{(k)}$ for $W(\hat{x}_i, x_{-i}^{(k)})$, $C_i(x_{-i}^{(k)})$, and $F_i(x_{-i}^{(k)})$, respectively, and denote the empirical conditional expectation $\mathbb{E} \left[W_i^{(k)\frac{1}{2}} (F_i^{(k)} \hat{x}_i - C_i^{(k)}) \middle| x_{-i}^{(k)} \right]$ of the weighted residuals by $\bar{R}^{(k)} = \mathbb{1} \frac{1}{M} \sum_{h=1}^M \sqrt{W_h(\hat{x}_i, x_{-i}^{(k)})} r_h(\hat{x}_i, x_{-i}^{(k)}) =$

$\frac{1}{M} \mathbb{1}^\top W_i^{(k)\frac{1}{2}} (F_i^{(k)} \hat{x}_i - C_i^{(k)})$, where $\mathbb{1} \in \mathbb{R}^M$ is the vector of all ones. Additionally, recall that, in general, $\text{Var} \neq \mathbb{V}$, as defined in Section 1.1.

Proposition 3 *Let $x_{-i}^{(k)}$ with $k = 1, \dots, N_S$ be samples generated from any distribution whose density never vanishes and is centered at the MLE. Under Assumption 1, one has*

$$\frac{\sum_{k=1}^{N_S} p^{(k)} \left((\sigma_i^{(k)})^2 (F_i^{(k)\top} W_i^{(k)} F_i^{(k)})^\dagger + F_i^{(k)\dagger} \bar{R}^{(k)} \bar{R}^{(k)\top} F_i^{(k)\dagger\top} \right)}{\sum_{k=1}^{N_S} p^{(k)}} - \frac{\sum_{k=1}^{N_S} p^{(k)} F_i^{(k)\dagger\top} \bar{R}_i^{(k)} \sum_{k=1}^{N_S} p^{(k)} \bar{R}_i^{(k)\top} F_i^{(k)\dagger\top}}{\sum_{k=1}^{N_S} p^{(k)}} \rightarrow \mathbb{V}[\hat{e}_i], \quad (22)$$

as $N_S \rightarrow \infty$ and where $p^{(k)} = \prod_{h=1}^M p_h(r_h(\hat{x}_i, x_{-i}^{(k)}))$ is the likelihood of a sample, and

$$\begin{aligned} (\sigma_i^{(k)})^2 &\equiv \text{Var} \left[W_i^{(k)\frac{1}{2}} (F_i^{(k)} \hat{x}_i - C_i^{(k)}) \right] \\ F_i^{(k)\dagger} &= \left(F_i^{(k)\top} W_i^{(k)} F_i^{(k)} \right)^\dagger F_i^{(k)\top} W_i^{(k)\frac{1}{2}}. \end{aligned}$$

Proof. First, we highlight that the variance of \hat{e}_i is generated by two different factors: the probability distributions p_h resulting in nonzero realizations of the residuals $r_h(\hat{x})$, and the uncertainty on the estimates \hat{x}_{-i} . Second, we observe that Algorithm 1 relies on the least squares fit of the weighted regression model $W_i^{(k)\frac{1}{2}} C_i^{(k)} = W_i^{(k)\frac{1}{2}} F_i^{(k)} \hat{x}_i^{(k)} + \varepsilon_i^{(k)}$. In this setting, the estimation error $\hat{e}_i^{(k)} = \hat{x}_i^{(k)} - x_i$ has an expectation and variance conditioned on $x_{-i}^{(k)}$ given by

$$\begin{aligned} \mathbb{E}[\hat{e}_i^{(k)} | x_{-i}^{(k)}] &= \mathbb{E}[\hat{x}_i^{(k)} - \hat{x}_i | x_{-i}^{(k)}] + \underbrace{\mathbb{E}[\hat{x}_i - x_i | x_{-i}^{(k)}]}_{=0}, \\ &= \underbrace{\mathbb{E}[\hat{x}_i^{(k)} - \hat{x}_i]}_{=0}, \\ &= \mathbb{E} \left[F_i^{(k)\dagger} W_i^{(k)\frac{1}{2}} (C_i^{(k)} - F_i^{(k)} \hat{x}_i) \middle| x_{-i}^{(k)} \right], \\ &= -F_i^{(k)\dagger} \bar{R}_i^{(k)}, \end{aligned} \quad (23a)$$

$$\begin{aligned} \mathbb{V}[\hat{e}_i^{(k)} | x_{-i}^{(k)}] &= F_i^{(k)\dagger\top} \text{Var} \left[W_i^{(k)\frac{1}{2}} (F_i^{(k)} \hat{x}_i - C_i^{(k)}) \right] F_i^{(k)\dagger}, \\ &= (\sigma_i^{(k)})^2 \left(F_i^{(k)\top} W_i^{(k)} F_i^{(k)} \right)^\dagger, \end{aligned} \quad (23b)$$

respectively. Finally, in order to compute the marginalized variance $\mathbb{V}[\hat{x}_i - x_i]$, one can use the Law of Total Variance (LTV) (Rudary, 2009)

$$\mathbb{V}[\hat{e}_i] = \mathbb{E} \left[\mathbb{V}[\hat{e}_i | x_{-i}^{(k)}] \right] + \mathbb{V} \left[\mathbb{E}[\hat{e}_i | x_{-i}^{(k)}] \right]. \quad (24)$$

The conditional (i.e., inner) variance and expectations is computed using (23), and as $N_S \rightarrow \infty$, the marginal (i.e., outer) ones can be obtained by using the empirical formulae

$$\mathbb{E}\left[\mathbb{V}\left[\hat{e}_i|x_{-i}^{(k)}\right]\right] = \frac{\sum_{k=1}^{N_S} p^{(k)} \mathbb{V}\left[\hat{e}_i^{(k)}|x_{-i}^{(k)}\right]}{\sum_{k=1}^{N_S} p^{(k)}}, \quad (25a)$$

$$\mathbb{V}\left[\mathbb{E}\left[\hat{e}_i|x_{-i}^{(k)}\right]\right] = \frac{\sum_{k=1}^{N_S} p^{(k)} \mathbb{E}\left[\hat{e}_i^{(k)}|x_{-i}^{(k)}\right] \mathbb{E}\left[\hat{e}_i^{(k)}|x_{-i}^{(k)}\right]^\top}{\sum_{k=1}^{N_S} p^{(k)}} \quad (25b)$$

Because $p^{(k)}$ appears in (25), the empirical variances become exact when the number of samples approaches infinity and their distribution is supported by $\mathbb{R}^{\sum_{j \neq i} n_j}$ (Kroese et al., 2013). Hence, one has (25a) + (25b) $\rightarrow \mathbb{V}[\hat{e}_i]$, which concludes the proof. \square

Requiring to compute a pseudoinverse for each sample k can be burdensome when N_S is large. In practice, the samples $x_{-i}^{(k)}$ have to be taken very close to the MLE \hat{x}_{-i} (i.e., where $p^{(k)} \ll \prod_{h=1}^M p_h(r_h(\hat{x}))$) to avoid having a small denominator in (22). Additionally, if the samples are close to the MLE, one has $F_i^{(k)} \approx F_i(\hat{x}_{-i})$. Thus, $F_i^{(k)\dagger}$ in (22) can be approximated using the first order Taylor expansion

$$\begin{aligned} (F_i^{(k)\top} W_i^{(k)} F_i^{(k)})^\dagger &\approx (F_i^\top(\hat{x}_{-i}) W_i F_i(\hat{x}_{-i}))^\dagger \\ &- \left(F_i^{(k)\top} W_i^{(k)} F_i^{(k)} - F_i^\top(\hat{x}_{-i}) W_i F_i(\hat{x}_{-i}) \right). \end{aligned} \quad (26)$$

The approximation, (26) improves the computational complexity significantly as only one pseudoinverse is needed for all samples. The accuracy of both (22) and (26) is discussed in Section 6.3.

6 Applications and experiments

In this section, we present four applications for AIRLS, which demonstrate the efficacy of AIRLS in terms of speed, scaling and robustness. We begin by considering specific instances of Examples 6 and 7 related to practical engineering problems. Moreover, we present two examples from economics and environmental science with more complex likelihoods, which highlights the broadness of problems that AIRLS can address.

6.1 Online system identification with outliers

In Brouillon et al. (2022b), AIRLS is applied to the error-in-variables online system identification problem of estimating the matrices $A \in \mathbb{R}^{n_x \times n_x}$, $B \in \mathbb{R}^{n_x \times n_u}$ in the system $x_{t+1} = Ax_t + Bu_t$ from noisy measurements of state and control variables

$$[\tilde{x}_t, \tilde{u}_t] = [x_t + \Delta x_t, u_t + \Delta u_t]. \quad (27)$$

To do so, we define the following data matrices

$$\begin{aligned} \tilde{C} &= \sum_{t=0}^T \beta^{T-t} \tilde{\Gamma}_t, \\ \tilde{Y} &= [I, 0_{n_x \times n_z}] \tilde{C} = E_y \tilde{C}, \quad : \tilde{\Gamma}_t = \begin{bmatrix} \tilde{x}_{t+1} \\ \tilde{x}_t \end{bmatrix} \begin{bmatrix} \tilde{x}_{t+1} \\ \tilde{x}_t \end{bmatrix}^\top, \\ \tilde{Z} &= [0_{n_z \times n_x}, I] \tilde{C} = E_z \tilde{C}, \quad \begin{bmatrix} \tilde{u}_t \\ \tilde{u}_t \end{bmatrix} \end{aligned} \quad (28)$$

where $n_z = n_x + n_u$ and $0 < \beta \leq 1$ is a forgetting factor. Given a prior Θ_0 , the identification task consists in estimating the parameters $\Theta = [A, B] \in \mathbb{R}^{n_x \times n_z}$ and the filtered measurements \hat{Z} such that $\Theta \hat{Z} - \tilde{Y}$, $\hat{Z} - \tilde{Z}$, and $\Theta - \Theta_0$ are Laplace-distributed and zero-expectation. This distribution provides a good robustness to outliers in the measurements $[\tilde{x}_t, \tilde{u}_t]$ (Brouillon et al., 2022b). The likelihood to maximize is therefore given by

$$\mathcal{L}(\Theta, Z | \tilde{Y}, \tilde{Z}, \Theta_0) = \prod_{h=1}^{n_x+n_z} \prod_{\ell=1}^{n_x} e^{-|\Theta_\ell Z_{:h} - \tilde{Y}_{:h}|} \cdot e^{-\frac{|Z_{:h} - \tilde{Z}_{:h}|}{n_x}} e^{-\frac{|\Theta_\ell - \Theta_{\ell,0}|}{n_x+n_z}}, \quad (29)$$

which is of the form (3). We compare the performance of the MLE of (29) computed with AIRLS to standard methods based on Gaussian distributions (i.e., subspace identification, Kalman filtering, and recursive total least squares) in Figure 1. The plot shows the relative parameter estimation error of the parameters of a two-dimensional system when a varying proportion of the state and input measurements is corrupted by outliers, which are uniformly distributed with a magnitude of 100% of each state's average value.

6.2 Matrix regression in power systems

The admittance matrix containing all the electrical parameters of a distribution grid is often not known by the operators. Identifying the admittance matrix automatically from voltage and current measurements allows for the optimization of the energy production without requiring too significant investments in modelling. The resulting estimates must however follow some characteristics common to all distribution grids such as sparsity (Ardakanian et al., 2019). Brouillon et al. (2022a) shows that the Bayesian EIV regression of the current on the voltage can produce sufficiently precise Maximum A Posteriori (MAP) estimates. In mathematical terms, this means that one must maximize the likelihood

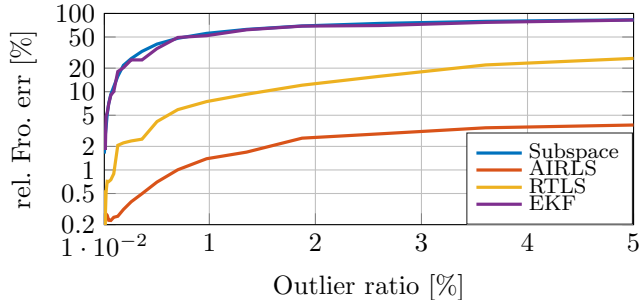


Fig. 1. Relative Frobenius error of the parameter estimates of a double-integrator system using 50 thousand samples for subspace identification (Van Overschee and De Moor, 1994), AIRLS, Recursive Total Least Squares (RTLS) (Rhode et al., 2014), and the Extended Kalman Filter (EKF) (Kullberg et al., 2021). The data has a proportion of outliers up to 5%. The vertical axis is in log scale.

$$\mathcal{L}(V, Y | \tilde{V}, \tilde{I}) = \prod_{h=1}^M e^{-\|\tilde{I}_h - VY_h\|_2^2} e^{-\|V_h - \tilde{V}_h\|_2^2} e^{-\|Y_h\|_1}, \quad (30)$$

where $V, I \in \mathbb{R}^{M \times N}$ are the nodal voltage and current data matrices containing N samples, their noisy observations are \tilde{V}, \tilde{I} , and $Y \in \mathbb{R}^{M \times M}$ is the admittance matrix to estimate. Figure 2 (from Brouillon et al. (2022a)) shows that the addition of the sparsity promoting prior in the MAP estimate provide a significant improvement over the MLE without this prior, which only uses Gaussian distributions. Moreover, Table 1 shows that AIRLS computes the MAP estimate (30) significantly faster than other methods adapted to the problem.

Table 1

Comparison of the execution speed of the Block Coordinate Descent (BCD) (Zhu et al., 2011), AIRLS, and ADMM (Boyd et al., 2011) to maximize (30) with $M = 9$ and $N = 400$.

Algorithm	iterations to convergence	iterations/second
BCD	~10000	1.25
AIRLS	~10000	30
ADMM	~30000	28

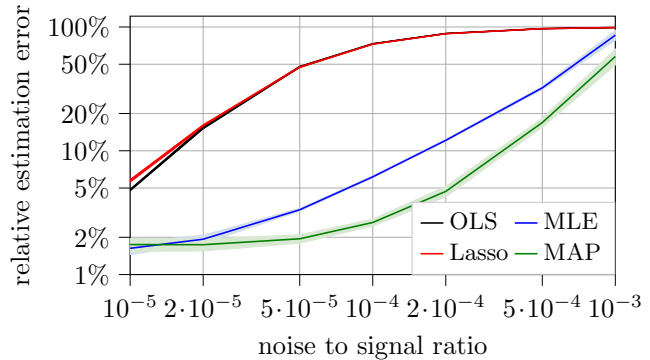


Fig. 2. Relative estimation error of power grid parameters using Ordinary Least Squares (OLS), Least Absolute Shrinkage and Selection Operator (Lasso), MLE, and MAP.

6.3 Economics supply demand problem

In this section, we compare various zeroth order optimization methods for the MLE of a graphical model for a supply-demand problem (e.g., for food harvest (Russell et al., 2010)). In this model, $S \in \mathbb{R}^T$ is the supply amounts of a good for $t = 1, \dots, T$ and $P \in \mathbb{R}^{n_T \times T}$ are the prices of n_T different suppliers at each time, which are modified by various taxes or subsidies $\tau \in \mathbb{R}^{n_T}$. This all leads to a demand $D \in \mathbb{R}^{n_T \times T}$, which corresponds to the quantities of the good that are sold by each seller for a price P_t . The model is defined by the following distributions, where the value of the parameters are chosen according to (Russell et al., 2010). Figure 3 represents this statistical model graphically as a Bayesian network.

$$p(S_t) \propto e^{-\left(\frac{(S_t - 100)^2}{200}\right)^{\frac{1}{5}}}, \quad (31a)$$

$$p(P_t | S_t, \tau) \propto e^{-\frac{\|(20 - 0.1S_t)\frac{1+0.01\tau}{n_T} - P_t\|_2^2}{0.02}}, \quad (31b)$$

$$p(D_t | P_t) \propto e^{-\frac{\|200 \cdot 1 - 10P_t - D_t\|_1}{\sqrt{2}}}. \quad (31c)$$

Moreover, $p(\tau)$ is a non-informative prior as defined in Syversveen (1998).

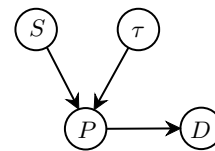


Fig. 3. Example of a supply demand Bayesian network model with taxes or subsidies.

To generate the data, we sample S_t over the prior distribution (31a), τ over a normal distribution around 10% with a standard deviation of 3%, and use the mode of (31b) and (31c) for P_t and D_t . In order to test Algorithm 1, we use the realizations of S_1, \dots, S_T and D_1, \dots, D_T to infer the values of P_1, \dots, P_T and τ .

The joint likelihood of a Bayesian network is given by the product of the conditional distributions of each node. Hence, because each distribution follows Assumption 1, the joint likelihood

$$\hat{P}, \hat{\tau} = \arg \min_{P_t, \tau} \prod_{t=1}^T \prod_{i \in \{a, b, c\}} (31i), \quad (32)$$

follows (3). This experiment is repeated 10 times. The solid lines in Figures 4, 5, 6, and 7 represent the average results, while the minimum and maximum are represented by shaded regions.

Convergence Speed: We use AIRLS and three benchmark zeroth order algorithms, i.e., discretization (Chen et al., 2017), sampling (Kroese et al., 2013), and zeroth order gradient descent (ZOGD) (Golovin et al., 2019), to solve (32). Figure 4 shows that, for this multiaffine problem, the convergence of AIRLS is much faster than all other algorithms.

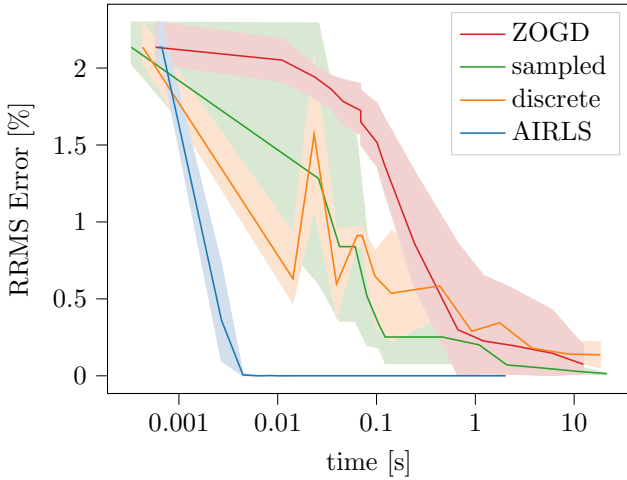


Fig. 4. Comparison of convergence speed of four algorithms for the inference of P_t in the example (31) with unknown τ , $T = 2$, and $n_T = 1$.

Scaling and robustness: When n_T or T increase, the sampling and discretization algorithms used in Figure 4 become very slow and unpractical. We therefore only compare ZOGD to AIRLS for illustrating the scaling of computational time with the dimensionality. Note that each iteration (9) of AIRLS relies on a least squares problem, which scales with $O(T^3)$. We do not provide a complexity bound for the number of iterations, but the following experiments show that the number of iterations increases only slightly in higher dimensions. Figure 5a shows this scaling compared to ZOGD.

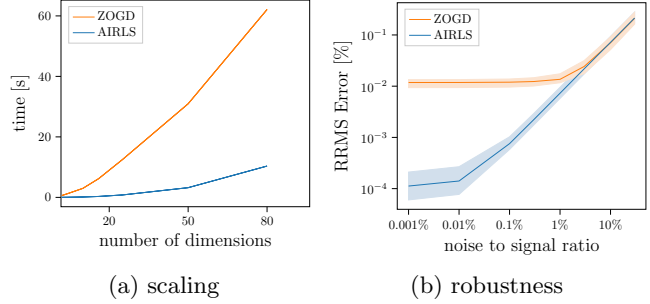


Fig. 5. Comparison of ZOGD and AIRLS for scaling with T , and for robustness to noise. The subfigures show (a) the computation time as a function of T and (b) the RRMS error of the estimate of P_t and τ depending on the average noise in S_t and D_t .

In practice, the chosen step size for ZOGD influences both its convergence speed and its accuracy. In this experiment, the step size for ZOGD is 0.99995^k , where k is the iteration number. This decreasing sequence obtained the best accuracy over all considered noise to signal ratios (see Figure 5b). In contrast, the accuracy of AIRLS only depends on α , which does not (or not directly) influence the convergence speed. This parameter is set to $\alpha = 10^{-3}$ in all experiments.

Convergence rate: In order to analyze the convergence speed of the algorithm, we increase the number of dimensions to $T = 4000$ and $n_T = 2$. This higher dimensionality increases the number of iterations required to reach convergence to 13, allowing us to plot the error trajectory with enough resolution in Figure 6. Additionally, Figure 6 shows that the convergence is super-linear, as the error decreases faster than $e_0 \cdot 0.7^k$ until it reaches the fixed point, where the error due to α is around 0.005%.

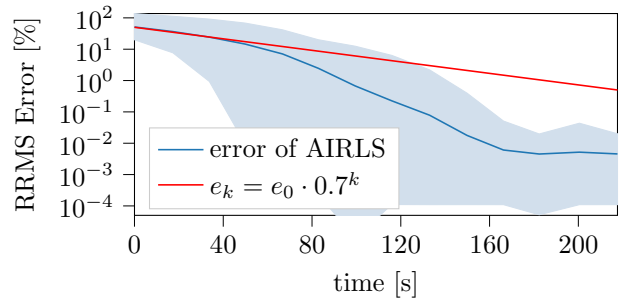


Fig. 6. Average error trajectory of AIRLS for the problem (31), and with $n_T = 2$ and $T = 4000$.

Variance estimation: We compare the variance computation (22) and its speed-up (26) for the example (31) to assess the accuracy of both methods in practice. The baseline used to compare the two estimates is generated by resampling the noise 10 times and using (21) on the results. Figure 7 shows that (22) is quite accurate, while (26) can be conservative for high noise levels.

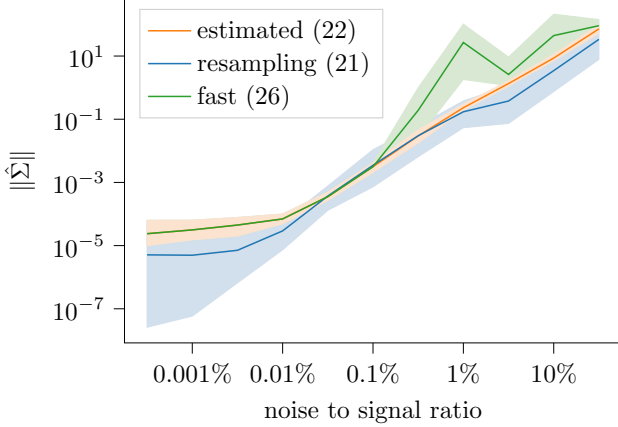


Fig. 7. Comparison of the spectral norms of covariance matrix estimates for various levels of noise, and using resampling (21), our estimator (22), and its faster approximation (26).

6.4 A complex example

As a last example, we describe a problem where all the aforementioned baseline methods fail to provide a meaningful estimate in a reasonable amount of time. We study a simplified model from (Newlands and Townley-Smith, 2010), which predicts the water usage by farms in a specific area. This model is defined by the following conditional probability distributions (33) and represented in graph form in Figure 8. Inference tasks associated with this model are much more challenging than for (31) due to the presence of log normal (33a) and asymmetric Laplace (33c) densities, as well as numerous relations between the variables.

In this model, the root nodes P_t and D_t are: (i) P_t the atmospheric pressure and (ii) $D_t = \sin^2\left(\frac{\pi}{365}t\right)$, which is a transformation of the day of the year. They influence the normalized sun irradiance I_t and the amounts of rain R_t . Finally, the amount of water W_t released by the system depends on the soil humidity H_t , which depends on the the sun irradiance in both present and past according to an auto-regressive model.

$$p(P_t) \propto e^{-\frac{\log(P_t)^2}{0.02}}, \quad (33a)$$

$$p(I_t|D_t) \propto e^{-105|I_t - D_t - 1| - 100(I_t - D_t - 1)}, \quad (33b)$$

$$p(R_t|P_t, D_t) \propto e^{-\frac{|(R_t - 3P_t(1 - D_t)) + 50(|R_t| - R_t)|}{3}}, \quad (33c)$$

$$p(H_t|I_t) \propto e^{-\frac{(H_t - 10 - \sum_{k=1}^t 0.9^{t-k} I_k)^2}{0.02}}, \quad (33d)$$

$$p(W_t|R_t, H_t) \propto e^{-\frac{(W_t - (H_t - R_t + 2))^2}{0.02}}. \quad (33e)$$

Moreover, D_t is exactly observed so we only introduce a non-informative prior (Syversveen, 1998) for $p(D_t)$.

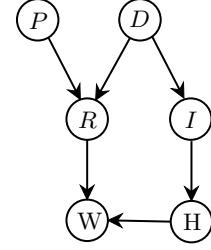


Fig. 8. Example of an environmental Bayesian network model for water use in agriculture.

We generate the data by sampling the distributions in (33) for each $t = 1, \dots, T$. The inference task consists in estimating R_t and I_t using the values of P_t , H_t , W_t , and D_t for all $t = 1, \dots, T$. The convergence speed and robustness to noisy data are shown in Fig. 9, where AIRLS shows a similar favorable performance as in Section 6.3. The comparison with ZOGD is absent because it converges too slowly.

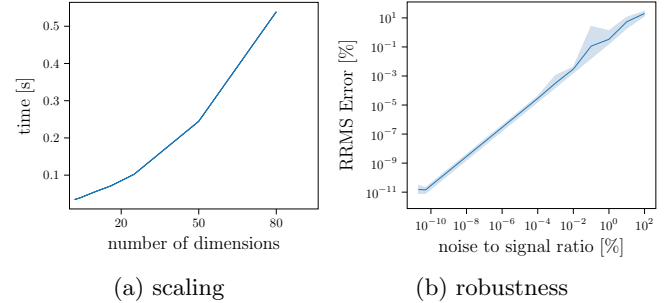


Fig. 9. Numerical results of Algorithm 1 applied to the example (33) for scaling with T , and for robustness to noise. The subfigures show (a) the computation time as a function of T and (b) the RRMS error of the estimate of R_t and I_t depending on the average noise in the other variables.

7 Conclusions

MLE problems are ubiquitous but can be very challenging to compute when some variables in the problem do not follow well-studied distributions. Moreover, state-of-the-art methods can be slow to solve high-dimensional problems. In this paper, we propose a simple likelihood optimization method, which converges for a wide variety of problems, and produces estimates very close to the optimum. We also provide an algorithm to compute the variance of these estimates efficiently, and show how to apply the whole method to a large class of statistical models.

While we provide a convergence proof and an optimality guarantee on the fixed points when all the variables follow GNDs, other classes of distributions will be investigated. Future work on AIRLS will also aim at characterizing the convergence speed analytically, in order to explain the empirically observed super-linear rate.

References

- Aleksandr Aravkin, James V Burke, Lennart Ljung, Aurelie Lozano, and Gianluigi Pillonetto. Generalized Kalman smoothing: Modeling and algorithms. *Automatica*, 86:63–86, 2017.
- O. Ardakanian, V. W. S. Wong, R. Dobbe, S. H. Low, A. von Meier, C. J. Tomlin, and Y. Yuan. On identification of distribution grids. *IEEE Transactions on Control of Network Systems*, 6(3):950–960, 2019.
- Amir Beck. *First-Order Methods in Optimization*. SIAM-Society for Industrial and Applied Mathematics, Philadelphia, PA, USA, 2017.
- Mónica Borunda, OA Jaramillo, Alberto Reyes, and Pablo H Ibarguengoytia. Bayesian networks in renewable energy systems: A bibliographical survey. *Renewable and Sustainable Energy Reviews*, 62:32–45, 2016.
- Giulio Bottegal, Aleksandr Y Aravkin, Håkan Hjalmarsson, and Gianluigi Pillonetto. Outlier robust system identification: A bayesian kernel-based approach. *IFAC Proceedings Volumes*, 47(3):1073–1078, 2014.
- Stephen Boyd, Neal Parikh, Eric Chu, Borja Peleato, and Jonathan Eckstein. Distributed optimization and statistical learning via the alternating direction method of multipliers. *Foundations and Trends in Machine Learning*, 3:1–122, 01 2011.
- Jean-Sebastien Brouillon. Cvblearn package. <https://github.com/DecodEPFL/CVBNlearn>, doi: 10.5281/zenodo.5725215, 2022.
- Jean-Sébastien Brouillon, Emanuele Fabbiani, Pulkit Nahata, Keith Moffat, Florian Dörfler, and Giancarlo Ferrari-Trecate. Bayesian error-in-variables models for the identification of distribution grids. *IEEE Transactions on Smart Grid*, 2022a.
- Jean-Sébastien Brouillon, Keith Moffat, Florian Dörfler, and Giancarlo Ferrari-Trecate. Robust online joint state/input/parameter estimation of linear systems. In *IEEE 61st Conference on Decision and Control (CDC)*, pages 2153–2158. IEEE, 2022b.
- Alessandro Carbonari, Massimo Vaccarini, and Alberto Giretti. Bayesian networks for supporting model based predictive control of smart buildings. *Dynamic programming and Bayesian inference, concepts and applications*, pages 1–15, 2014.
- Yi-Chun Chen, Tim A Wheeler, and Mykel J Kochenderfer. Learning discrete bayesian networks from continuous data. *Journal of Artificial Intelligence Research*, 59:103–132, 2017.
- Alessandro Chiuso. Regularization and Bayesian learning in dynamical systems: Past, present and future. *Annual Reviews in Control*, 41:24–38, 2016.
- Evrin Dalkiran and Hanif Sherali. RLT-POS: Reformulation-linearization technique-based optimization software for solving polynomial programming problems. *Mathematical Programming Computation*, 8, 02 2016.
- Jan de Leeuw. Block-relaxation algorithms in statistics. In Hans-Hermann Bock, Wolfgang Lenski, and Michael M. Richter, editors, *Information Systems and Data Analysis*, pages 308–324, Berlin, Heidelberg, 1994. Springer Berlin Heidelberg.
- Stuart Gibson and Brett Ninness. Robust maximum-likelihood estimation of multivariable dynamic systems. *Automatica*, 41(10):1667–1682, 2005.
- Daniel Golovin, John Karro, Greg Kochanski, Chansoo Lee, Xingyou Song, and Qiuyi Zhang. Gradientless descent: High-dimensional zeroth-order optimization. *arXiv preprint arXiv:1911.06317*, 2019.
- Zvi Griliches, Michael D Intriligator, Robert Engle, and Dan McFadden. *Handbook of econometrics*. Elsevier, 1983.
- Rajarshi Guhaniyogi, Shaan Qamar, and David B. Dunson. Bayesian tensor regression. *Journal of Machine Learning Research*, 18(79):1–31, 2017.
- Scott Hellman, Amy McGovern, and Ming Xue. Learning ensembles of continuous bayesian networks: An application to rainfall prediction. In *2012 Conference on Intelligent Data Understanding*, pages 112–117. IEEE, 2012.
- Zhen Hu and Sankaran Mahadevan. Bayesian network learning for data-driven design. *ASCE-ASME J Risk and Uncert in Engrg Sys Part B Mech Engrg*, 4(4), 2018.
- Dirk P Kroese, Thomas Taimre, and Zdravko I Botev. *Handbook of monte carlo methods*. John Wiley & Sons, 2013.
- Anton Kullberg, Isaac Skog, and Gustaf Hendeby. Online joint state inference and learning of partially unknown state-space models. *IEEE Transactions on Signal Processing*, 69:4149–4161, 2021.
- C. Kümmerle, C. M. Verdun, and Dominik Stöger. Iteratively reweighted least squares for ℓ_1 -minimization with global linear convergence rate. *ArXiv*, abs/2012.12250, 2020.
- Erich L Lehmann and George Casella. *Theory of point estimation*. Springer Science & Business Media, 2006.
- George Livadiotis. General fitting methods based on lq norms and their optimization. *Stats*, 3(1):16–31, 2020.
- Carlos Llosa. Tensor on tensor regression with tensor normal errors and tensor network states on the regression parameter. *Creative Components*, 82, 2018.
- Paolo Magni, Riccardo Bellazzi, and Giuseppe De Nicolao. Bayesian function learning using MCMC methods. *IEEE Transactions on Pattern Analysis and Machine Intelligence*, 20(12):1319–1331, 1998.
- Michael J McGeachie, Hsun-Hsien Chang, and Scott T Weiss. Cgbayesnets: conditional gaussian bayesian network learning and inference with mixed discrete and continuous data. *PLoS computational biology*, 10(6):e1003676, 2014.
- Stefano Monti and Gregory F Cooper. A multivariate discretization method for learning Bayesian networks from mixed data. *arXiv preprint arXiv:1301.7403*, 2013.
- Kevin P Murphy. *Machine learning: a probabilistic perspective*. MIT press, 2012.
- Saralees Nadarajah. A generalized normal distribution. *Journal of Applied statistics*, 32(7):685–694, 2005.

Nathaniel K Newlands and Lawrence Townley-Smith. Predicting energy crop yield using bayesian networks. In *Proceedings of the fifth IASTED international conference*, volume 711, pages 014–106, 2010.

Brett Ninness and Soren Henriksen. Bayesian system identification via markov chain monte carlo techniques. *Automatica*, 46(1):40–51, 2010.

Farnaz Nojavan, Song S Qian, and Craig A Stow. Comparative analysis of discretization methods in bayesian networks. *Environmental Modelling & Software*, 87: 64–71, 2017.

Miguel Picallo, Saverio Bolognani, and Florian Dörfler. Sensitivity conditioning: Beyond singular perturbation for control design on multiple time scales. *IEEE Transactions on Automatic Control*, 68(4):2309–2324, 2022.

Song S Qian and Robert J Miltner. A continuous variable bayesian networks model for water quality modeling: A case study of setting nitrogen criterion for small rivers and streams in ohio, usa. *Environmental Modelling & Software*, 69:14–22, 2015.

Stephan Rhode, Felix Bleimund, and Frank Gauterin. Recursive generalized total least squares with noise covariance estimation. *IFAC Proceedings Volumes*, 19, 08 2014.

Matthew R Rudary. *On predictive linear gaussian models*. University of Michigan, 2009.

S. Russell, S.J. Russell, P. Norvig, and E. Davis. *Artificial Intelligence: A Modern Approach*. Prentice Hall series in artificial intelligence. Prentice Hall, 2010.

Lawrence K Saul. A tractable latent variable model for nonlinear dimensionality reduction. *Proceedings of the National Academy of Sciences*, 117(27):15403–15408, 2020.

Torsten Söderström. *Errors-in-variables methods in system identification*. Springer, 2018.

Anne Syversveen. Noninformative bayesian priors. interpretation and problems with construction and applications. *Preprint statistics 3*, pages 1–11, 03 1998.

Peter Van Overschee and Bart De Moor. N4sid: Subspace algorithms for the identification of combined deterministic-stochastic systems. *Automatica*, 30(1): 75–93, 1994. Special issue on statistical signal processing and control.

Rene Vidal, Yi Ma, and Shankar Sastry. Generalized principal component analysis (gpca). *IEEE transactions on pattern analysis and machine intelligence*, 27(12):1945–1959, 2005.

Ning Xu, Timothy CG Fisher, and Jian Hong. Instrument variable detection with graph learning: an application to high dimensional gis-census data for house pricing. *arXiv preprint arXiv:2007.15769*, 2020.

Hua Zhou, Lexin Li, and Hongtu Zhu. Tensor regression with applications in neuroimaging data analysis. *Journal of the American Statistical Association*, 108: 540–552, 06 2013.

Hao Zhu, Geert Leus, and G.B. Giannakis. Sparsity-cognizant total least-squares for perturbed compressive sampling. *Signal Processing, IEEE Transactions*

on, 59:2002 – 2016, 06 2011.

Appendix

Details of Example 5

Vidal et al. (2005) provides an expression for the fitting problem in the stochastic case. With all points ϕ_h corrupted by i.i.d. Gaussian noise, the problem is written as

$$\arg \min_{x_1, \dots, x_n} \sum_{h=1}^M \prod_{i=1}^n (\phi_h^\top x_i)^2 = \arg \max_{x_1, \dots, x_n} - \sum_{h=1}^M \prod_{i=1}^n (\phi_h^\top x_i)^2,$$

or equivalently

$$\begin{aligned} \arg \max_{x_1, \dots, x_n} \sum_{h=1}^M \ln \left(e^{-\left(\prod_{i=1}^n \phi_h^\top x_i\right)^2} \right) \\ = \arg \max_{x_1, \dots, x_n} \ln \left(\prod_{h=1}^M e^{-\left(\prod_{i=1}^n \phi_h^\top x_i\right)^2} \right). \end{aligned} \quad (34)$$

Taking the exponential of (34) does not change the optimizers x_1, \dots, x_n . With $p(\cdot) = \sqrt{\pi^{-1}} e^{-\left(\cdot\right)^2}$, (34) is therefore equivalent to the problem given in Example 5.

Details of Examples 6 and 7

Both examples are constituted of two matrices of measurements Z_1 and Z_2 , whose noises are assumed to be independent. In Example 6, one tries to fit (i) $Z_2 = X_1 X_0 + \varepsilon_0$ and (ii) $X_1 = Z_1 + \varepsilon_1$, where each element $\varepsilon_{0th} = Z_{2th} - \sum_{i=1}^n X_{1ti} X_{0ih}$ and $\varepsilon_{1th} = X_{1th} - Z_{1th}$ of the matrices ε_0 and ε_1 have density p_{0th} and p_{1th} , respectively. In this case, the joint likelihood is equal to

$$\prod_{t=1}^T \prod_{h=1}^n p_{0th}(\varepsilon_{0th}) p_{1th}(\varepsilon_{1th})$$

Plugging each elements of the matrix regression models (i) and (ii) yields the maximum likelihood shown in Example 6. Note that when all elements of ε_0 and ε_1 are Gaussian and i.i.d., the negative log-likelihood has the well-known form

$$\|Z_2 - X_1 X_0\|_F^2 + \|X_1 - Z_1\|_F^2.$$

Example 7 only contains one regression problem $Z = \Phi X + \varepsilon$. However, as tensors can get quite high dimensional, the parameter X is often constrained to have a certain rank. This can be done by expression X as the product of smaller-sized tensors. For simplicity, consider 2-dimensional tensors, i.e., matrices. If $X \in \mathbb{R}^{n \times n}$, any X of rank $r \leq n$ can be expressed as $X = X_1 X_2$, where

$X_1 \in \mathbb{R}^{n \times r}$ and $X_2 \in \mathbb{R}^{r \times n}$. This gives the regression $Z = \Phi X_1 X_2 + \varepsilon$, where each element of the noise ε_{th} is distributed according to the density p_{th} . Plugging this regression model element-wise into (3) yields the MLE problem given in Example 7.

This figure "network.png" is available in "png" format from:

<http://arxiv.org/ps/2409.03495v1>

This figure "y_bus.png" is available in "png" format from:

<http://arxiv.org/ps/2409.03495v1>

This figure "y_mle.png" is available in "png" format from:

<http://arxiv.org/ps/2409.03495v1>

This figure "y_tls.png" is available in "png" format from:

<http://arxiv.org/ps/2409.03495v1>